Check for updates

ADVANCED OPTICAL MATERIALS
www.advopticalmat.de

Polarization-Sensitive and Self-Driven Pyro-Phototronic Photodetectors Based on MoS_2-Water Heterojunctions

*Amin Abnavi, Ribwar Ahmadi, Hamidreza Ghanbari, Mirette Fawzy, Mohammad Reza Mohammadzadeh, Fahmid Kabir, and Michael M. Adachi**

Polarization-sensitive and self-driven pyroelectric-based photodetectors have recently gained interest due to their potential application in artificial electronic eyes, biomedical imaging, and optical switches. Here, a photodetector based on light modulation-induced polarization and depolarization of water molecules on the surface of a 2D MoS_2 crystal is reported. The MoS_2-water heterostructure photodetector serves as a self-driven pyro-phototronic device that converts light-induced thermal energy to electrical signals, leading to a transient photoresponsivity as high as 24.6 mA W^{-1} and a specific detectivity of 2.85 × 10^8 Jones under 470 nm wavelength at zero bias. Due to the formation of a built-in electric field at the MoS_2-water interface, this structure also has a high steady–state responsivity of 3.62 A W^{-1} and detectivity of 9.18 × 10^8 Jones at 3 V bias, along with a fast response time of ≈0.74 ms. Moreover, due to the rearrangement of the hydrogen bond network in the liquid water upon visible light illumination, the MoS_2-water photodetector is light polarization-sensitive. The simple fabrication process, low cost, polarization sensitivity, and high performance of the MoS_2-water structure make it an excellent candidate for liquid-compatible photodetectors.

1. Introduction

Photodiodes are widely utilized across various industries including telecommunications,[1] imaging,[2] medical treatment,[3] and environmental sensing.[4] Among various materials, 2D transition metal dichalcogenides (TMDs), such as MoS_2, have gained attention as promising photodetector materials due to their exceptional material properties, including high visible light absorption,[5–6] superior flexibility,[7] low thickness,[8] and high electron mobility.[9–10]

Conventional photodetectors require an external voltage bias which can limit their applications due to energy consumption and extra cost.[11] p-n junction photodiodes are commonly used to obtain photocurrent at zero bias but are difficult to achieve in atomically thin TMDs due to the challenges of doping 2D materials or requiring transfer techniques to form heterojunctions.[12–14] Photodetectors based on the pyroelectric effect are a new type of photodetector that can detect light signals by converting light-induced thermal energy to electrical energy, which can enhance the transient response of the device.[11] A pyro-phototronic photodetector can use the combined effects of both the steady–state photovoltaic and transient pyroelectric responses at zero bias.[15–16]

In addition, polarization sensitivity is a crucial feature for photodetectors due to their applications in various fields such as navigation,[17] biomedical imaging,[18] and optical switches.[11] One way to create polarization-sensitive photodetectors is by using materials with anisotropic crystal structures such as black phosphorus,[18] TiS_3,[19] and WS_2.[20] However, 2D MoS_2 crystals are not responsive to light polarization, making it necessary to find new methods to develop MoS_2-based polarization-sensitive photodetectors.[21] For example, polarization sensitivity can be achieved through the use of heterostructures between MoS_2 and anisotropic materials such as GeSe,[18] $ReSe_2$,[22] and Te,[23] or by using the rolling-up technique.[21] Despite the potential benefits, the fabrication of such structures is challenging due to the complexity of the fabrication process and 2D material transfer methods.[13]

Recently, it has been shown that centrosymmetric materials can exhibit pyroelectricity at the interface with other materials.[24–25] For instance, we previously reported that a silicon-water heterostructure can be used for self-driven and polarization-sensitive photodetectors based on the interfacial pyroelectric effect.[11] Light-induced excitation of the hydrogen bond network in water, including those in the terahertz (THz) regime, creates anisotropy and polarization sensitivity in water.[26–27] Additionally, water and silicon can create a

A. Abnavi, R. Ahmadi, H. Ghanbari, M. R. Mohammadzadeh, F. Kabir, M. M. Adachi
School of Engineering Science
Simon Fraser University
8888 University Drive, Burnaby, British Columbia V5A 1S6, Canada
E-mail: mmadachi@sfu.ca
M. Fawzy
Department of Physics
Simon Fraser University
8888 University Drive, Burnaby, British Columbia V5A 1S6, Canada

The ORCID identification number(s) for the author(s) of this article can be found under https://doi.org/10.1002/adom.202302651

© 2024 The Authors. Advanced Optical Materials published by Wiley-VCH GmbH. This is an open access article under the terms of the Creative Commons Attribution License, which permits use, distribution and reproduction in any medium, provided the original work is properly cited.

DOI: 10.1002/adom.202302651

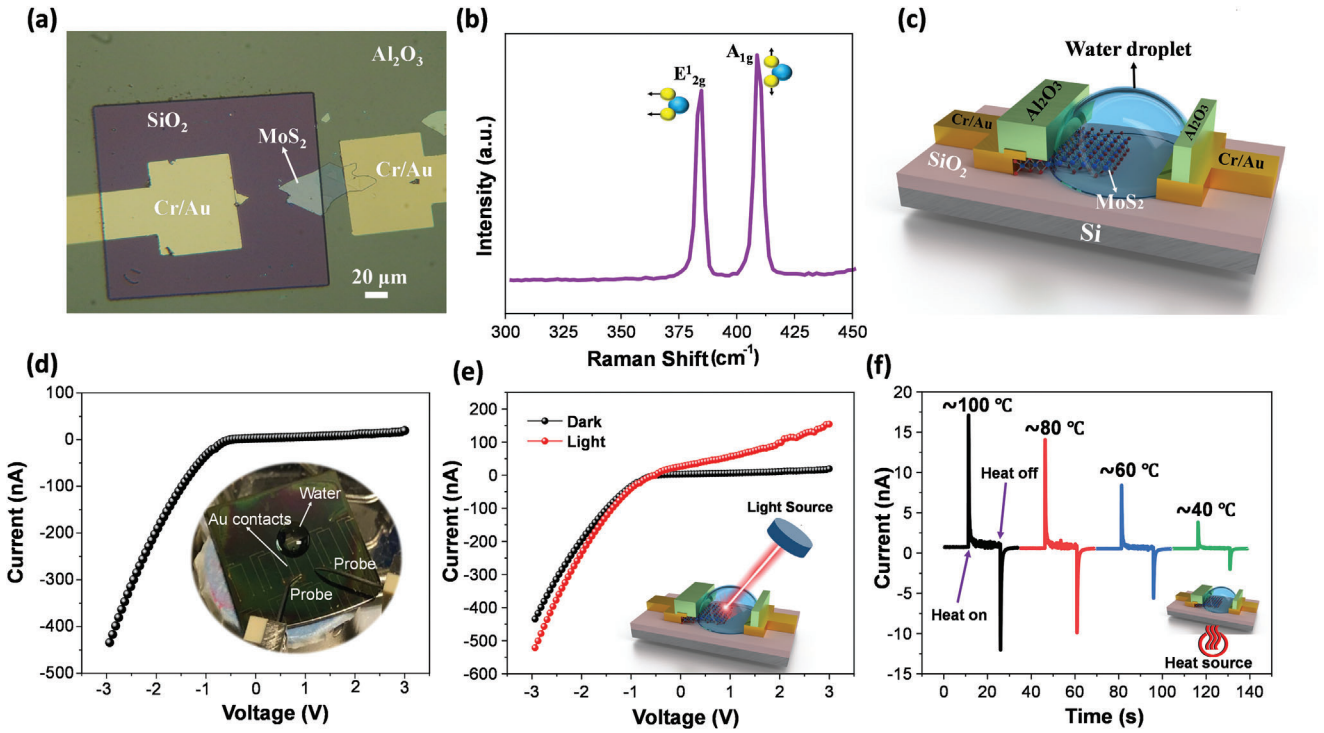

Figure 1. Structural, electrical, optical, and thermal characterization of the MoS_2-water heterostructure device. a) The optical image of the fabricated structure before placing the water droplet on it. b) Raman spectroscopy of the MoS_2 crystal, indicating the semiconducting 2H phase. c) Schematic of the MoS_2-water heterostructure device. d) The I-V characteristics of the MoS_2-water heterostructure device at dark conditions. The inset shows the actual MoS_2-water device in a chamber during the measurement. Note that the MoS_2 crystal is electrically grounded. e) The I-V characteristics of the MoS_2-water device at dark and light conditions (Solar spectrum AM1.5G, 100 mW cm^{-2}), showing the photovoltaic effect. f) The pyroelectric current of the MoS_2-water device when multiple heat pulses are applied to the back of MoS_2-water structure using a heat source.

heterojunction due to energy band bending at the interface.[11,28–29] The polar water molecules can form an ordered structure on a hydrophilic semiconductor surface, which can lead to pyroelectric behavior in water.[30–33] However, silicon has an indirect bandgap and is rigid and brittle, which can limit its use in flexible wearables and biomedical optoelectronic applications. Here, by using the ultrahigh visible light absorption of MoS_2,[34] and the formation of a heterojunction between MoS_2 and water, a self-driven and polarization-sensitive pyro-phototronic MoS_2-water photodetector is reported. This heterostructure photodetector shows a transient photoresponsivity as high as 24.6 mA W^{-1} and a specific detectivity of 2.85×10^8 Jones under 470 nm wavelength at zero bias. It also shows a high steady–state responsivity of 3.62 A W^{-1} with a detectivity of 9.18×10^8 Jones at 3 V bias, along with the fast rise/fall times of ≈0.741/2.83 ms. The combination of the simple fabrication process and high performance makes the MoS_2-water heterojunction an attractive candidate for dual steady–state and transient type photodetectors.

2. Results and Discussion

The MoS_2-water heterojunction consists of two Cr/Au electrodes, one of which overlaps a mechanically exfoliated multilayer MoS_2 crystal. A thin film of Al_2O_3 is used to electrically passivate one electrode, and a window is created to expose MoS_2 to air. The fabrication process is illustrated in Figures S1 and S2 (Supporting Information). **Figure** 1a presents the optical image of the fabricated MoS_2-based structure from the top view, which displays a portion of the MoS_2 flake and one of the Cr/Au electrodes exposed to air. The Raman spectroscopy of the MoS_2 crystal shows two sharp peaks, the in-plane mode (E_{2g}) at ≈384 cm^{-1} and the out-of-plane mode (A_{1g}) at 408 cm^{-1} (Figure 1b). This confirms that the MoS_2 flake is in a semiconducting phase (2H-phase) as previously reported.[34] Finally, 50 µL deionized (DI) water is placed on the active area so that one Cr/Au electrode is connected to DI water and the other one is connected to the MoS_2 crystal, forming a MoS_2-water heterostructure device, as schematically shown in Figure 1c. Figure 1d shows the linear scale current-voltage (I–V) characteristics of the MoS_2-water device under dark conditions, demonstrating a current rectification ratio, defined as the current ratio at ±1 V, of ≈22 without a gate voltage. This rectification behavior is due to an internal electric field formed by an energy band bending at the interface between MoS_2 and water. The inset of Figure 1d shows the actual MoS_2-water device connected to two probes in a chamber during the measurement. Figure 1e shows the I–V characteristics of the MoS_2-water heterostructure under dark and light irradiation. The energy band diagrams of water and MoS_2 when they are separate and in contact are illustrated in Figure S3 (Supporting Information). The energy band structure of water has previously been reported in triboelectric studies at the silicon-water interfaces.[28,35] To determine the band bending at the MoS_2-water interface, we also examined the optoelectronic and electronic behavior of n-type and p-type silicon-water heterojunctions. The Fermi level of n-type silicon is

© 2024 The Authors. Advanced Optical Materials published by Wiley-VCH GmbH

21951071, 0, Downloaded from https://onlinelibrary.wiley.com/doi/10.1002/adom.202302651 by Simon Fraser University, Wiley Online Library on [07/02/2024]. See the Terms and Conditions (https://onlinelibrary.wiley.com/terms-and-conditions) on Wiley Online Library for rules of use; OA articles are governed by the applicable Creative Commons License

higher than that of water due to the high electron concentration which results in the transfer of electrons to the water upon physical contact, leading to the band bending at the interface[28] (Figure S4a,b, Supporting Information). This band bending results in a diode-like rectifying behavior in the IV characteristics of silicon-water heterojunction (Figure S4c, Supporting Information). On the other hand, the electrons transfer from water to p-type silicon, resulting in a different band bending and IV characteristics[35] (i.e., opposite polarity) (Figure S4d–f, Supporting Information). Although MoS_2 is typically an n-type semiconductor, the IV characteristics and band bending of MoS_2-water heterojunction are similar to those of p-type silicon-water probably due to the low electron concentration of MoS_2.[36]

Upon white light illumination (solar spectrum, AM1.5G) at an intensity of 100 mW cm^{-2}, the concentration of photogenerated carriers in the MoS_2 increases, leading to an increase in the photogenerated current density of the MoS_2-water device and an open circuit voltage of ≈0.52 V, demonstrating the photovoltaic effect[37] (Figure 1e). To study the pyroelectric behavior of the MoS_2-water junction, a series of heat pulses at temperatures of ≈40, 60, 80, and 100 °C were applied to the backside of the MoS_2-water device (Figure 1f). When a heat pulse is applied to the device, a short-duration positive current peak is generated due to the depolarization of water dipoles on the MoS_2 surface. A built-in electric field at the MoS_2-water interface facilitates the collection of pyroelectric charges at zero bias, leading to a sharp spike in current response due to the incident light turning on and off. During steady–state heating, the positive peak quickly declines to near zero due to a decrease in temperature gradient over time. When the heat pulse is removed, a negative current peak is generated that similarly dissipates quickly (Figure 1f). Therefore, heating and cooling generate pyroelectric currents in opposite directions.

Due to the lack of net orientation, water on its own has minimal or no pyroelectricity.[32] However, it has been shown that the alignment of polarized water molecules can exhibit crystalline properties and pyroelectric behavior. For example, pyroelectric behavior has been observed in electrically biased water ice[32] and silicon-water heterojunctions.[11] Similar to pyroelectric materials such as $BaTiO_3$ (BTO),[38] there is a linear relationship between the transient current and the change in temperature (ΔT) for the MoS_2-water heterojunction device (Figure S5, Supporting Information).

The MoS_2-water heterojunction exhibits a light-induced pyroelectric effect in the configuration illustrated in **Figure 2a**, which can be used for photodetection. When a light pulse is applied, the photodetector response measured between the two Au contacts consists of transient peaks generated due to the pyroelectric effect in addition to a steady–state current generated by the photovoltaic effect.[39] The self-driven transient photocurrent of the MoS_2-water device under 470 nm wavelength light at different intensities of 1.5–6.8 mW cm^{-2} are shown in Figure 2b, showing distinguishable transient responses for different light intensities due to polarization and depolarization of water molecules on the surface of MoS_2 crystal as the incident light is turned on and off. The amplitude of the positive transient peaks is plotted as a function of light intensity in Figure 2c. Under zero-bias conditions, the steady–state photocurrent is low compared to the transient photocurrent. To further assess the photodetection performance of MoS_2-water photodetector, two critical parameters, responsivity (R), and detectivity (D), are calculated using the following equations:[40]

$$R = \frac{I_{ph}}{PS} \tag{1}$$

$$D = \frac{RS^{\frac{1}{2}}}{\left(2eI_d\right)^{\frac{1}{2}}} \tag{2}$$

where $I_{ph} = |I_{light}|-|I_{dark}|$ is the photocurrent amplitude, P is the incident light intensity, I_d is the dark current, e is the charge of an electron and S is the effective surface area of the MoS_2-water interface, which is ≈904 μm^2 (Figure S6, Supporting Information). The detectivity of a photodetector measures its ability to detect weak light signals and the responsivity measures the photocurrent generated per input optical power. Figure 2d shows the transient responsivity and detectivity of the MoS_2-water heterojunction where the photocurrent (I_{ph}) is the amplitude of the positive transient peak. The highest transient responsivity and detectivity of 24.6 mA W^{-1} and 2.85 × 10^8 Jones are achieved at the lowest light intensity of 1.5 mW cm^{-2}, respectively. Both the transient responsivity and detectivity decrease as a function of increasing the light intensity, which may be attributed to electron trap saturation and an increase in electron–hole recombination.[41] The photoresponse rise and fall times of the MoS_2-water device at zero bias were also measured to be ≈3.2 and ≈150 ms, respectively (Figure 2e). The transmission spectrum of water on a glass substrate reveals a high transmission of ≈95% at a wavelength of 470 nm (Figure S7, Supporting Information). We have also previously reported that the water-MoS_2 device demonstrates a reflectance of ≈3.5% at the same wavelength.[36] Therefore, the absorption of water is minimal at this specific wavelength.

MoS_2 on its own is not a polarization-sensitive material due to its isotropic structure. In fact, two factors are likely responsible for the polarization sensitivity of MoS_2-water photodetector. First, light reflection at the water surface is polarization-dependent, as shown in the reflectance spectrum on the surface of water-glass (Figure S8, Supporting Information). Second, the terahertz frequency range, including the visible spectrum, can rearrange the hydrogen bonds, stimulate water molecules, and generate anisotropy,[26–27,42] leading to polarization sensitivity. The photoresponse of the MoS_2-water photodetector at different polarization angles is demonstrated in Figure 2f. The polarization angle was controlled by passing natural light with a wavelength of 470 nm through a rotation-controllable crystal polarizer (Inset of Figure 2f). Figure 2g shows the polar plot of the MoS_2-water device for different polarization angles of 0–360°, showing distinguishable transient photocurrents at different angles. The polarization sensitivity of the MoS_2-water device makes it suitable for many applications including artificial electronic eyes,[11] biomedical imaging,[18] and optical switches.[11]

Compared to previously reported self-powered pyro-phototronic photodetectors, listed in **Table 1**, the MoS_2-water heterojunction offers a simple fabrication process, high responsivity, and polarization sensitivity. Additionally, the MoS_2-water heterojunctions can be used for the development of flexible and

© 2024 The Authors. Advanced Optical Materials published by Wiley-VCH GmbH

21951071, 0, Downloaded from https://onlinelibrary.wiley.com/doi/10.1002/adom.202302651 by Simon Fraser University, Wiley Online Library on [07/02/2024]. See the Terms and Conditions (https://onlinelibrary.wiley.com/terms-and-conditions) on Wiley Online Library for rules of use; OA articles are governed by the applicable Creative Commons License

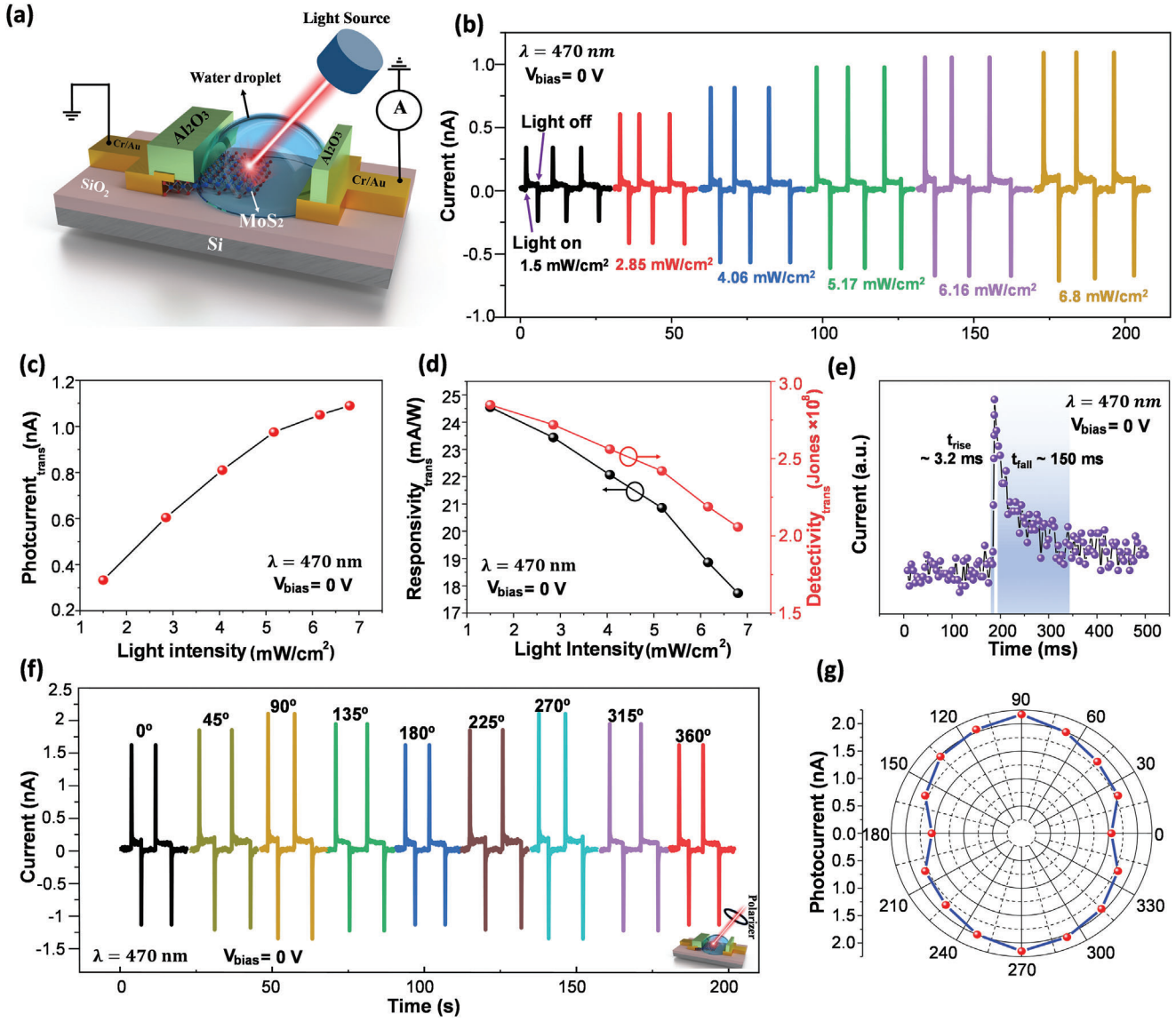

Figure 2. Self-driven photodetection characterization of the MoS_2-water heterostructure device. a) Schematic illustration of the MoS_2-water heterostructure photodetector. Note that the electrode connected to MoS_2 is electrically grounded. b) Photoresponse of the MoS_2-water device at multiple light intensities of 1.5, 2.85, 4.06, 5.17, 6.16, and 6.8 mW cm^{-2} at zero bias. The wavelength of light is 470 nm. c) The transient photocurrent of the MoS_2-water device as a function of light intensity (1.5–6.8 mW cm^{-2}). d) Transient responsivity and detectivity of the MoS_2-water device as a function of light intensity (1.5–6.8 mW cm^{-2}). e) The photoresponse rise/fall times of the MoS_2-water device at zero bias. f) The photoresponse of the MoS_2-water device at different polarization angles. g) Polar plot of the MoS_2-water device under a natural light (λ = 470 nm) as a function of polarization angle, showing polarization sensitivity.

lightweight photodetectors that can be integrated into various devices and systems due to the excellent mechanical flexibility of 2D MoS_2.[7]

Although the steady–state photocurrent amplitude is negligible compared to the transient photocurrent at zero bias, it can increase significantly at larger bias voltages due to the enhanced collection of the photogenerated electron/holes.[54] The schematic of the MoS_2-water photodetector under bias voltages is shown in **Figure 3**a. Figure 3b–f shows the photoresponse of the photodetector to incident light (λ = 470 nm, light intensity = 6.8 mW cm^{-2}) under different bias voltage conditions of 0, 0.5, 1, 2, and 3 V, respectively. At each bias voltage, the incident light was turned on and off three times to show the repeatability of the photoresponse. By increasing the bias voltage, the amplitude of the transient current peak decreases, which may be due to the weakening of the pyroelectric effect due to joule heating induced by the applied bias voltage.[39] The steady–state photocurrent increases from ≈97 pA to ≈223 nA when increasing the bias voltage from 0 to 3 V (Figure 3g), resulting in an enhancement of the steady–state responsivity from 1.58 to 3628 mA W^{-1} (Figure 3h). The steady–state detectivity also enhances from 1.86×10^7 to 9.18×10^8 Jones with increasing bias voltage (Figure 3h). The

© 2024 The Authors. Advanced Optical Materials published by Wiley-VCH GmbH

21951071, 0, Downloaded from https://onlinelibrary.wiley.com/doi/10.1002/adom.202302651 by Simon Fraser University, Wiley Online Library on [07/02/2024]. See the Terms and Conditions (https://onlinelibrary.wiley.com/terms-and-conditions) on Wiley Online Library for rules of use; OA articles are governed by the applicable Creative Commons License

Table 1. Comparison between the MoS2-water photodetector with other self-powered pyro-phototronic photodetectors in terms of light polarization sensitivity, wavelength (λ), light intensity, response time, and responsivity.

Device Structure	Polarization Sensitivity [Yes/No]	λ [nm]	Light Intensity [mW cm^{-2}]	Response time	Maximum Responsivity [mA W^{-1}]	Reference
ZnO:Ga/GaN	No	370	0.11	44 ms	>5	[43]
Si/SnO_x/ZnO	No	405	36.3	3 µs	36.7	[44]
NiO/ZnO	No	365	0.43	3.92 µs	0.29	[15]
ZnO/Si	No	325	0.03	19 µs	8.32	[45]
SnS/Si	No	760	7	12 µs	13	[46]
V_2O_5/ZnO	No	365	4	4 µs	36.34	[47]
Cl:ZnO/PEDOT:PSS	No	365	0.3	28 ms	2.33	[48]
ZnO/Spiro-MeOTAD	No	365	1	160 ms	0.8	[49]
Ag-ZnO	No	325	0.00034	25.87 ms	0.047	[50]
ZnO/CuSCN	No	380	6	4 ns	7.5	[51]
ZnO/perovskite	No	325	0.019	53 µs	26.7	[52]
Si/ perovskite	No	780	0.013	40 ms	1.5	[53]
Si-water	Yes	400	0.006	20 ms	754	[11]
MoS_2-water	Yes	470	1.5	3.2 ms	24.6	This Work

Table 2. Comparison between the MoS_2-water photodetector with other polarization-sensitive MoS_2-based heterostructure photodetectors in terms of mechanism, wavelength (λ), applied bias voltage, response time, and responsivity.

Structure	Mechanism/ effect	λ [nm]	Bias Voltage [V]	Response time [ms]	Maximum responsivity [mA W^{-1}]	Reference
GaTe/MoS_2	Steady–state/ Photovoltaic	532	$V_{ds} = 2V_g = -40$	10	145	[55]
GaAs/MoS_2	Steady–state/ Photovoltaic	780	0	0.0034	35.2	[56]
SWCNT–MoS_2	Steady–state/ Photovoltaic	532	0	102	0.1	[57]
GeSe/MoS_2	Steady–state/ Photovoltaic	532	0	110	105	[18]
Folded MoS_2	Steady–state/ Photovoltaic	660	1	690	100	[21]
$ReSe_2$/MoS_2	Steady–state/ Photovoltaic	638	4	0.005	3520	[22]
MoS_2-water	Transient/ Pyroelectric	470	0	≈3.2	24.6	This work
MoS_2-water	Steady–state/ Photovoltaic	470	3	≈0.74	3628	This work

photoresponse rise/fall times are ≈0.741/≈2.83 ms at a bias voltage of 3 V (Figure 3i), showing the suitability of the MoS_2-water photodetector for high-speed optoelectronic applications.

A comparison of the MoS_2-water photodetector and other polarization-sensitive MoS_2-based photodetectors reported in the literature is summarized in **Table 2**. The MoS_2-water photodetector device benefits from high responsivity, a simple fabrication process, and compatibility for applications that involve an aqueous environment.

To examine the effect of water volume on the photoresponse of the MoS_2-water device, different amounts of DI water droplets (5, 20, 40, and 80 µL) were used and the photoresponses were recorded (Figure S9, Supporting Information). Both steady–state and transient photocurrents decrease with increasing the size of the water droplet, which could be due to the water curvature-dependent reflection of light on the water surface. We also observed that the photoresponse is highly dependent on the incident light angle (Figure S10, Supporting Information). The maximum photocurrent is achieved when the incident light is normal to the sensor surface (incident light angle of 90°), which could be due to the incident angle-dependent reflection at the water surface and change in light intensity. Therefore, the steady–state and transient photocurrents highly depend on the curvature of a water droplet and incident light angle.

The physical mechanism of the pyro-phototronic effect at the MoS_2-water interface is described using a four-stage photoresponse process illustrated in **Figure 4**. In stage 1, the light is turned on, inducing both pyroelectric and photovoltaic effects (Figure 4a). In this stage, the photogenerated electrons in the MoS_2 flow from MoS_2 to water due to band bending at the MoS_2-water interface (Figure 4b). De-polarization of water molecules on the surface of the MoS_2 crystal and the presence of a built-in electric field at the MoS_2-water interface result in a large transient pyroelectric current peak when the light is turned on (Figure 4c). In stage 2, when the incident light has been on for a period of time, the pyroelectric current disappears due to the device reaching an equilibrium temperature and only the photocurrent due to the photovoltaic effect remains (Figure 4d). Figure 4e shows the band-diagram during this stage and the flow of photo-generated electrons from MoS_2 to water due to the built-in electric field at the MoS_2-water interface, resulting in the generation of a steady–state photocurrent (Figure 4f). Note that this steady–state photocurrent enhances significantly when a non-zero bias voltage is applied across the MoS_2-water device (Figure 3g). In stage 3

© 2024 The Authors. Advanced Optical Materials published by Wiley-VCH GmbH

21951071, 0, Downloaded from https://onlinelibrary.wiley.com/doi/10.1002/adom.202302651 by Simon Fraser University, Wiley Online Library on [07/02/2024]. See the Terms and Conditions (https://onlinelibrary.wiley.com/terms-and-conditions) on Wiley Online Library for rules of use; OA articles are governed by the applicable Creative Commons License

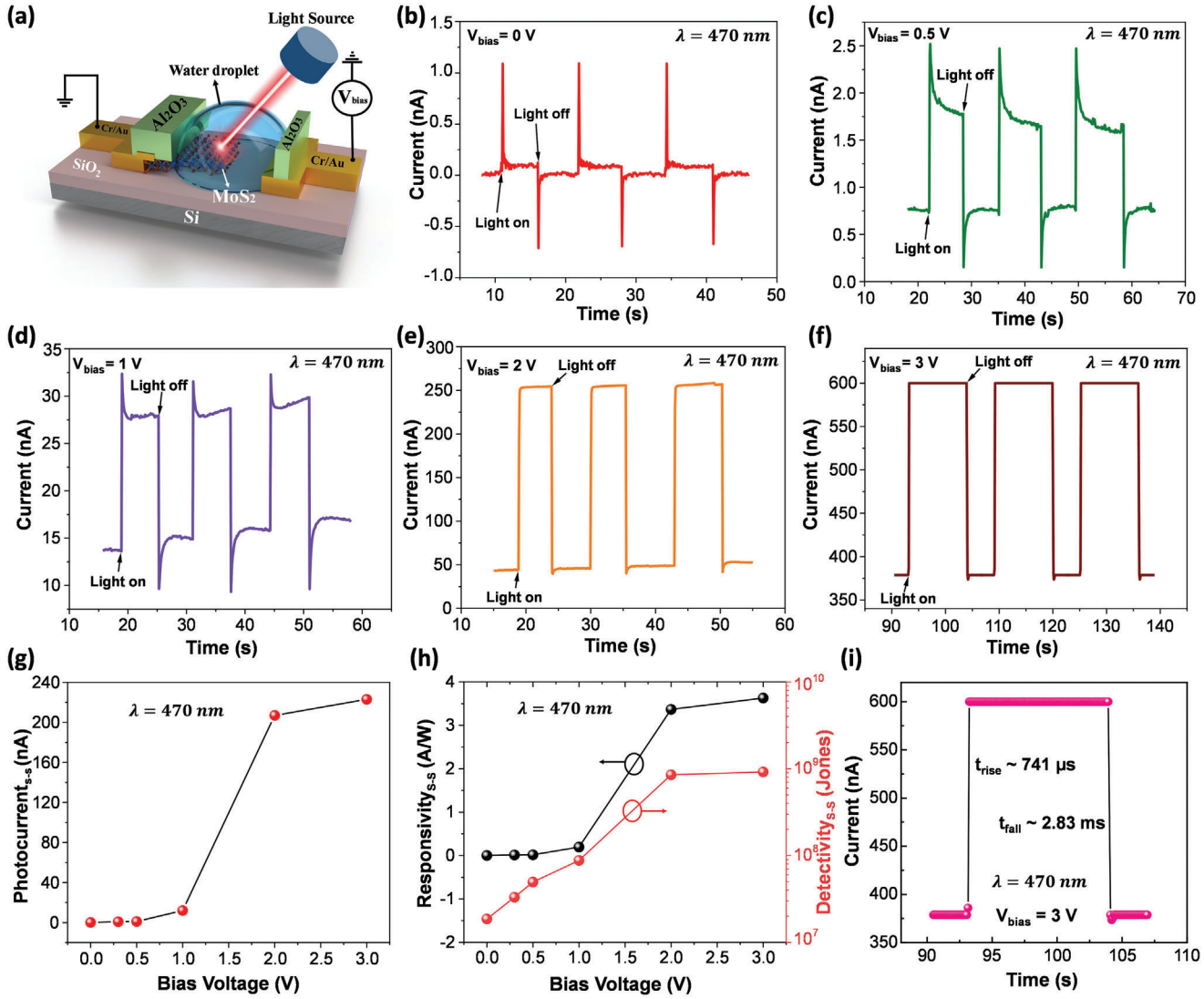

Figure 3. The effect of bias voltage on the photoresponse. a) The schematic of the MoS_2-water photodetector under different bias voltages. The photoresponse of the MoS_2-water device under different bias voltages of b) 0, c) 0.5, d) 1, e) 2, and f) 3 V with the same light intensity of 6.8 mW cm^{-2}. g) The steady–state photocurrent of the MoS_2-water device under different bias voltages of 0–3 V at the same light intensity of 6.8 mW cm^{-2}. h) The steady–state responsivity and detectivity of the MoS_2-water device under different bias voltages of 0–3 V at the same light intensity of 6.8 mW cm^{-2}. i) The photoresponse rise/fall times of the MoS_2-water device at a bias voltage of 3 V.

(Figure 4g–i), the incident light is turned off, and a transient pyroelectric current peak with negative polarity, opposite to that of stage 1, is generated due to the device cooling down and fast polarization of water molecules on the MoS_2 (Figure 4g). The band diagram illustrating a flow of electrons from water to MoS_2 during this stage is shown in Figure 4h. In the absence of incident light, the photocurrent is generated only by the pyroelectric effect and has no steady-steady photovoltaic component (Figure 4i). After a period of time without incident light, the pyroelectric effect disappears, and the current returns to about zero, as shown in stage 4 (Figure 4j–l). The photoresponse characteristics and energy band structure of the MoS_2-water heterojunction in relation to the n-type and p-type silicon-water heterostructures are illustrated in Figure S11 (Supporting Information). The photoresponse in MoS_2-water structure is similar to that of p-type silicon-water due to the similar orientation of water molecules at their surfaces.

DI water was used as the liquid in this study and H_2O being a polar molecule is critical for the generation of pyroelectric currents at the MoS_2-liquid interface. Replacing DI water with toluene, a non-polar solvent, results in no pyroelectric effect and therefore no transient current upon light illumination (Figure S12, Supporting Information). The equilibrium state of ordered water molecules on the MoS_2 substrate is schematically illustrated in **Figure 5a**. When a change in temperature is induced by light, dipoles are excited, raising their energy levels, causing a deviation from the mean equilibrium ordered position and a reduction in the electrical dipole moment (Figure 5b). This results in the release of electrons/holes that move to the external circuit, generating a transient current response. Immediately thereafter,

© 2024 The Authors. Advanced Optical Materials published by Wiley-VCH GmbH

21951071, 0, Downloaded from https://onlinelibrary.wiley.com/doi/10.1002/adom.202302651 by Simon Fraser University, Wiley Online Library on [07/02/2024]. See the Terms and Conditions (https://onlinelibrary.wiley.com/terms-and-conditions) on Wiley Online Library for rules of use; OA articles are governed by the applicable Creative Commons License

21951071, 0, Downloaded from https://onlinelibrary.wiley.com/doi/10.1002/adom.202302651 by Simon Fraser University, Wiley Online Library on [07/02/2024]. See the Terms and Conditions (https://onlinelibrary.wiley.com/terms-and-conditions) on Wiley Online Library for rules of use; OA articles are governed by the applicable Creative Commons License

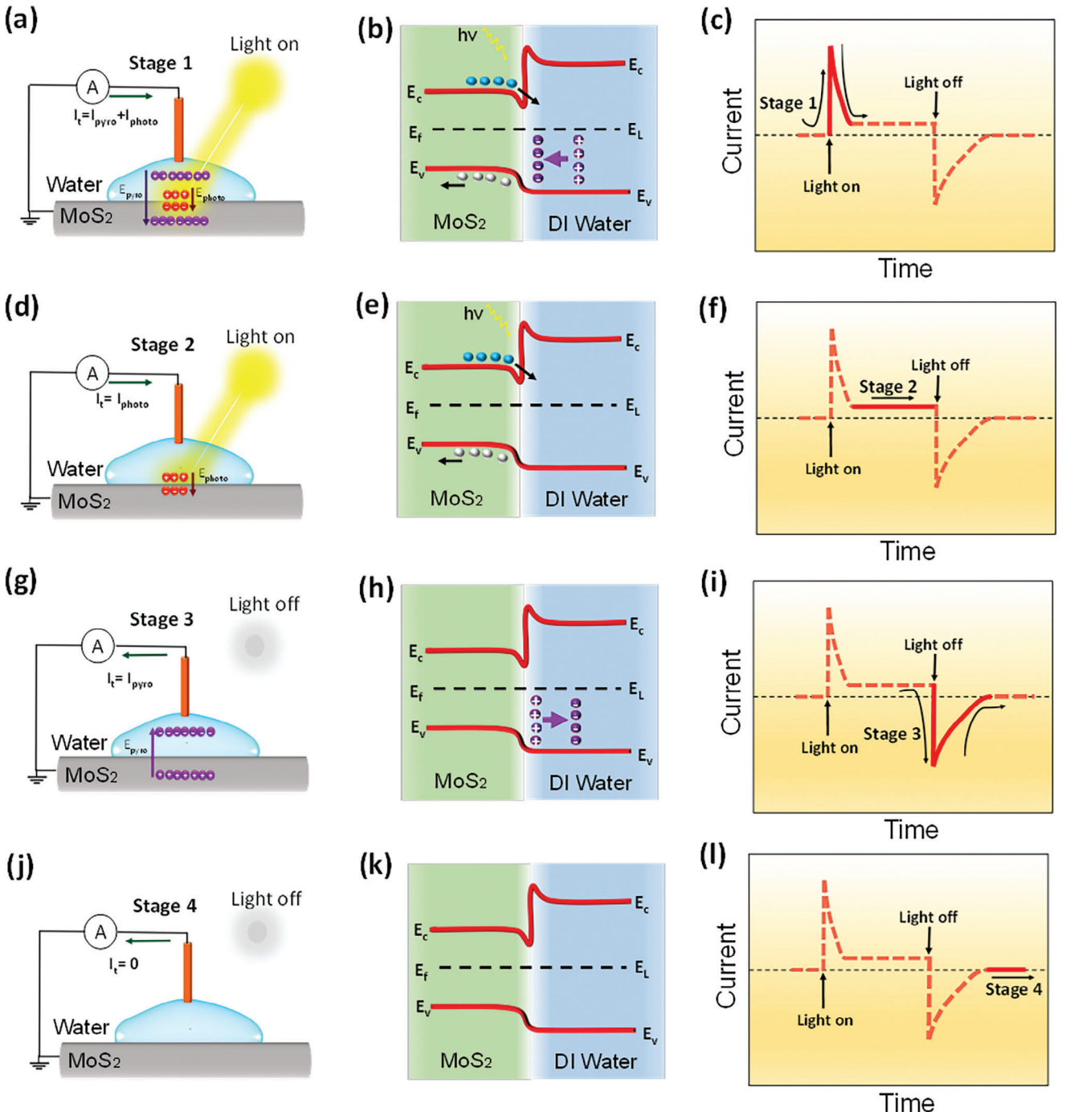

Figure 4. Working mechanism of the MoS_2-water pyro-phototronic photodetector. a–c) Stage 1: when the incident light is turned on, both pyroelectric and photovoltaic currents are present, which results in a large transient response. d–f) Stage 2: when the incident light is kept on for some time: the pyroelectric current disappears due to the lack of temperature gradient and there is only steady–state photovoltaic current. g–i) Stage 3: when the incident light is turned off, a pyroelectric current in the opposite direction is generated due to the temperature gradient. j–l) Stage 4: after the light remains off for a moment, both pyroelectric and photovoltaic currents disappear and the current returns to zero.

the lattice of water molecules re-forms, producing an equivalent current in the opposite direction.

The frequency-dependent photocurrent of the MoS_2-water under a square-wave light signal was measured at different frequencies. The measurement setup consists of a function generator-powered LED ($\lambda = 470$ nm, 50% duty cycle) and an oscilloscope to measure the MoS_2-water heterostructure photoresponse across a 15 MΩ resistor is illustrated in **Figure** 6a. The MoS_2-water photocurrent as a function of light at frequencies between 1 Hz and 100 kHz is shown in Figure 6b. At low frequencies (1–10 Hz),

© 2024 The Authors. Advanced Optical Materials published by Wiley-VCH GmbH

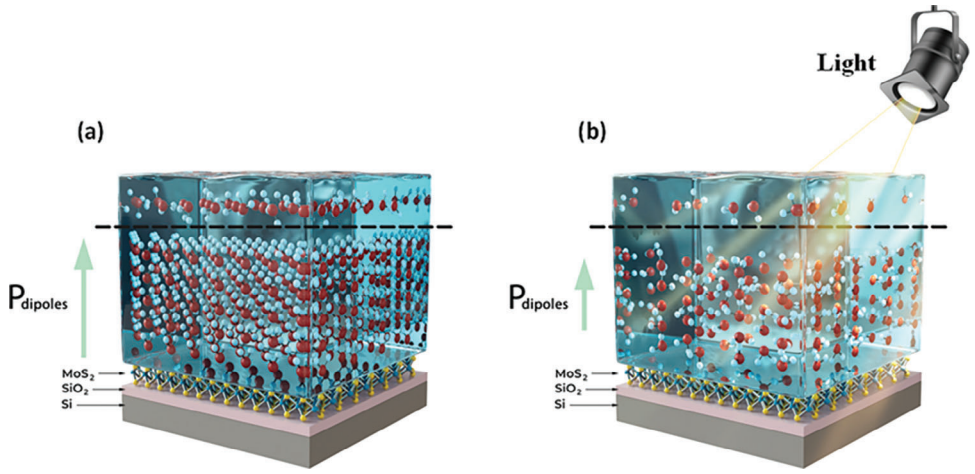

Figure 5. Working mechanism of the MoS_2-water photodetector. a) The equilibrium position state of ordered water molecules on the MoS_2. b) The excitation of dipoles under light illumination and reduction in the electrical dipole moment.

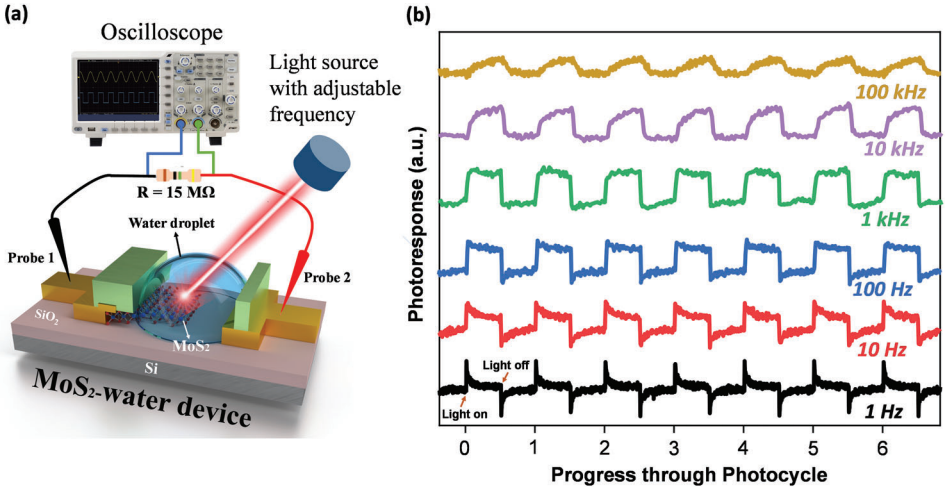

Figure 6. The light frequency-dependent photoresponse of the MoS_2-water device. a) The setup schematic for measuring the frequency-dependent photoresponse. b) Frequency-dependent photoresponse of the MoS_2-water device tested in the air with light pulse frequencies from 1 Hz to 100 kHz and $V_{bias} = 0$ ($\lambda = 470$ nm).

the device has enough time for complete capacitive charging and therefore both transient and steady–state responses are visible. As the frequency increases and the time interval between two consecutive pulses is lower than the rise time of the device, the transient response diminishes, resulting in semi-square wave photocurrents. This square-shaped response is maintained up to a frequency of ~10 kHz and the maximum detectable frequency is ~100 kHz. The distinguishable photoresponses over a wide range of frequencies make the MoS_2-water photodetectors suitable for high-frequency optoelectronic applications.

In this work, to fabricate MoS_2-water heterojunction devices, we used mechanically exfoliated MoS_2 flakes, and the DI water droplet was drop-casted on the structure as a proof-of-concept photodetector device. A major disadvantage of using exfoliated flakes is that we do not have control over the dimension, thickness, and shape of the flakes. Furthermore, water droplet shape, curvature, and amount cannot be accurately controlled in this method, resulting in varying photoresponses from device to device. To expand this proof-of-concept to an array of MoS_2-water photodetectors on a single chip, large-area 2D MoS_2 can be produced through chemical vapor deposition (CVD)[58] or wet chemical processes,[59] etched in rectangular shapes, and transparent polymers (e.g., PDMS) or conductive 2D materials (e.g., graphene) can be deployed to encapsulate the water.[60] The simple fabrication process, self-driven capability, fast response, and polarization sensitivity make the MoS_2-water structure an excellent candidate for optoelectronic applications.

3. Conclusion

Here, the MoS_2-water heterostructure has been demonstrated for self-driven and polarization-sensitive photodetection applications. The pyroelectric response is based on the polarization and depolarization of water molecules on the MoS_2 surface.

© 2024 The Authors. Advanced Optical Materials published by Wiley-VCH GmbH

21951071, 0, Downloaded from https://onlinelibrary.wiley.com/doi/10.1002/adom.202302651 by Simon Fraser University, Wiley Online Library on [07/02/2024]. See the Terms and Conditions (https://onlinelibrary.wiley.com/terms-and-conditions) on Wiley Online Library for rules of use; OA articles are governed by the applicable Creative Commons License

The MoS_2-water photodetector illustrates a transient photoresponsivity as high as 24.6 mA W^{-1} and a specific detectivity of 2.85×10^8 Jones under 470 nm at zero bias. It also shows a high steady–state responsivity of 3.62 A W^{-1} with a high detectivity of 9.18×10^8 Jones at 3 V bias, along with the rise/fall times of ≈0.741/2.83 ms. The simplicity, low cost, and high performance of the MoS_2-water structure make it an excellent candidate for liquid-compatible photodetectors.

4. Experimental Section

Device Preparation: MoS_2 flakes were mechanically exfoliated from a bulk MoS_2 crystal (SPI Supplies) using Nitto SPV224 tape and transferred onto a p-type (100) Si wafer coated with thermally oxidized 300 nm SiO_2. Cr/Au (10/60 nm) electrodes were patterned by photolithography in a way that one electrode is on the MoS_2 crystal, followed by the thermal evaporation and the lift-off process in an acetone bath. Al_2O_3 (40 nm) was deposited on the device using an atomic layer deposition (ALD) system. Then, a window was opened on the device in a way that part of the MoS_2 crystal and the second electrode was exposed to air using photolithography and wet etching by buffered oxide etchant (BOE) 6:1 solution. The substrate was then cleaned using acetone, IPA, and DI water. Finally, a 50 µL water droplet was placed on the exposed MoS_2 flake. The fabrication process is shown in Figures S1 and S2 (Supporting Information).

Material Characterization: The structure of the MoS_2 device was characterized by Optical Microscopy. The Raman spectra of the MoS_2 device were recorded on a Renishaw inVia a confocal Raman microscope equipped with a 514 nm continuous-wave excitation laser.

Electrical/Optical Characterization: Electrical measurements were performed using a Keithley 2400 source meter at room temperature. The Si substrate was not contacted and left electrically floating. For the photodetection measurements, an LED with an adjustable intensity and a wavelength of 470 nm was utilized. For the rise/fall time and frequency-dependent photoresponse measurements, the MoS_2-water photodetector was illuminated with a 470 nm LED powered by a function generator (Tektronix AFG3151C). The MoS_2-water device was connected in series to a resistor (15 MΩ), and an oscilloscope (Tektronix MDO3104) was used to measure the voltage across the resistor. All measurements were conducted at atmospheric pressure and room temperature.

Supporting Information

Supporting Information is available from the Wiley Online Library or from the author.

Acknowledgements

This work was supported by the Natural Sciences and Engineering Research Council of Canada (NSERC), Canada Foundation for Innovation (CFI), British Columbia Knowledge Development Fund (BCKDF), Western Economic Diversification Canada (WD), and Simon Fraser University. The authors thank B. Kim for maintenance of the SFU Engineering Science cleanroom facility, Dr. D. Leznoff for access to Raman microscopy, and Mr. Ehsan Faridi for designing the figures schematics. The authors acknowledge CMC Microsystems and 4D LABS shared facilities that facilitated this research.

Conflict of Interest

The authors declare no conflict of interest.

Author Contributions

A.A. and R.A. contributed equally to this work. A.A. and R.A. performed all experimental design, fabrication, and measurements under the supervision of M.M.A. H.G. participated in device fabrication, data analysis, and scientific discussions. M.F., M.R.M., and F.K. participated in data analysis and scientific discussions. M.M.A. supervised the project and assisted with data analysis and manuscript preparation.

Data Availability Statement

The data that support the findings of this study are available from the corresponding author upon reasonable request.

Keywords

interfacial pyroelectricity, liquid-semiconductor optoelectronic, MoS_2-water photodetector, polarization-sensitive photodetector, pyro-phototronic photodetector

Received: October 18, 2023
Revised: December 20, 2023
Published online:

[1] L. H. Zeng, S. H. Lin, Z. J. Li, Z. X. Zhang, T. F. Zhang, C. Xie, C. H. Mak, Y. Chai, S. P. Lau, L. B. Luo, *Adv. Funct. Mater.* **2018**, *28*, 1705970.
[2] W. Gao, S. Zhang, F. Zhang, P. Wen, L. Zhang, Y. Sun, H. Chen, Z. Zheng, M. Yang, D. Luo, *Adv. Electron. Mater.* **2021**, *7*, 2000964.
[3] M. J. Large, J. A. Posar, A. J. Mozer, A. Nattestad, S. Alnaghy, M. Carolan, P. J. Sellin, J. Davies, Z. Pastuovic, M. L. Lerch, *ACS Appl. Mater. Interfaces* **2021**, *13*, 57703.
[4] R. Eckstein, T. Rödlmeier, T. Glaser, S. Valouch, R. Mauer, U. Lemmer, G. Hernandez-Sosa, *Adv. Electron. Mater.* **2015**, *1*, 1500101.
[5] Y. Liu, Y.-X. Yu, W.-D. Zhang, *J. Phys. Chem. C* **2013**, *117*, 12949.
[6] K. Alkanad, A. Hezam, Q. A. Drmosh, S. S. Ganganakatte Chandrashekar, A. A. AlObaid, I. Warad, M. A. Bajiri, L. Neratur Krishnappagowda, *Sol. RRL* **2021**, *5*, 2100501.
[7] W. Li, M. Xu, J. Gao, X. Zhang, H. Huang, R. Zhao, X. Zhu, Y. Yang, L. Luo, M. Chen, *Adv. Mater.* **2023**, *35*, 2207447.
[8] A. Splendiani, L. Sun, Y. Zhang, T. Li, J. Kim, C.-Y. Chim, G. Galli, F. Wang, *Nano Lett.* **2010**, *10*, 1271.
[9] N. P. Rezende, A. R. Cadore, A. C. Gadelha, C. L. Pereira, V. Ornelas, K. Watanabe, T. Taniguchi, A. S. Ferlauto, A. Malachias, L. C. Campos, *Adv. Electron. Mater.* **2019**, *5*, 1800591.
[10] X. Feng, Y. Li, L. Wang, S. Chen, Z. G. Yu, W. C. Tan, N. Macadam, G. Hu, L. Huang, L. Chen, *Adv. Electron. Mater.* **2019**, *5*, 1900740.
[11] R. Ahmadi, A. Abnavi, H. Ghanbari, H. Mohandes, M. R. Mohammadzadeh, T. De Silva, A. Hasani, M. Fawzy, F. Kabir, M. M. Adachi, *Nano Energy* **2022**, *98*, 107285.
[12] J. Jiang, Y. Wen, H. Wang, L. Yin, R. Cheng, C. Liu, L. Feng, J. He, *Adv. Electron. Mater.* **2021**, *7*, 2001125.
[13] A. J. Watson, W. Lu, M. H. Guimarães, M. Stöhr, *2D Mater.* **2021**, *8*, 032001.
[14] Y. Xiao, C. Li, X. Tan, L. Zhang, Y. Zhong, H. Zhu, *Sol. RRL* **2017**, *1*, 1700135.
[15] A. K. Rana, M. Kumar, D. K. Ban, C. P. Wong, J. Yi, J. Kim, *Adv. Electron. Mater.* **2019**, *5*, 1900438.
[16] Y. Zhang, M. Hu, Z. Wang, *Nano Energy* **2020**, *71*, 104630.
[17] P. Wan, M. Jiang, L. Su, S. Xia, Y. Wei, T. Xu, Y. Liu, D. Shi, X. Fang, C. Kan, *Adv. Funct. Mater.* **2022**, *32*, 2207688.
[18] Y. Xin, X. Wang, Z. Chen, D. Weller, Y. Wang, L. Shi, X. Ma, C. Ding, W. Li, S. Guo, *ACS Appl. Mater. Interfaces* **2020**, *12*, 15406.

© 2024 The Authors. Advanced Optical Materials published by Wiley-VCH GmbH

21951071, 0, Downloaded from https://onlinelibrary.wiley.com/doi/10.1002/adom.202302651 by Simon Fraser University, Wiley Online Library on [07/02/2024]. See the Terms and Conditions (https://onlinelibrary.wiley.com/terms-and-conditions) on Wiley Online Library for rules of use; OA articles are governed by the applicable Creative Commons License

[19] J. Wang, C. Jiang, W. Li, X. Xiao, *Adv. Opt. Mater.* **2022**, *10*, 2102436.
[20] E. Wu, D. Wu, C. Jia, Y. Wang, H. Yuan, L. Zeng, T. Xu, Z. Shi, Y. Tian, X. Li, *ACS Photonics* **2019**, *6*, 565.
[21] T. Deng, S. Li, Y. Li, Y. Zhang, J. Sun, W. Yin, W. Wu, M. Zhu, Y. Wang, Z. Liu, *Nanophotonics* **2020**, *9*, 4719.
[22] K. Li, C. Du, H. Gao, T. Yin, Y. Yu, W. Wang, *J. Materiomics* **2022**, *8*, 1158.
[23] J. Yao, F. Chen, J. Li, J. Du, D. Wu, Y. Tian, C. Zhang, J. Yang, X. Li, P. Lin, *J. Mater. Chem. C* **2021**, *9*, 13123.
[24] M.-M. Yang, Z.-D. Luo, Z. Mi, J. Zhao, S. P. E., M. Alexe, *Nature* **2020**, *584*, 377.
[25] L. Guo, H. Wang, Z. Xu, R. Cong, L. Zhao, S. Zhang, K. Zhang, L. Gao, S. Wang, C. Pan, *Adv. Funct. Mater.* **2023**, *33*, 2306526.
[26] K. Ramasesha, S. T. Roberts, R. A. Nicodemus, A. Mandal, A. Tokmakoff, *J. Chem. Phys.* **2011**, *135*, 054509.
[27] F. Novelli, L. Ruiz Pestana, K. C. Bennett, F. Sebastiani, E. M. Adams, N. Stavrias, T. Ockelmann, A. Colchero, C. Hoberg, G. Schwaab, *J. Phys. Chem. B* **2020**, *124*, 4989.
[28] M. Zheng, S. Lin, Z. Tang, Y. Feng, Z. L. Wang, *Nano Energy* **2021**, *83*, 105810.
[29] Y. Yan, Y. Lu, C. Liu, X. Yu, C. Wang, R. Yang, S. Lin, *Sol. RRL* **2022**, *6*, 2200782.
[30] L. Chen, X. He, H. Liu, L. Qian, S. H. Kim, *J. Phys. Chem. C* **2018**, *122*, 11385.
[31] J. Zhou, H. Li, L. Zhao, R. Chow, *Canadian J. Chem. Eng.* **2018**, *96*, 1986.
[32] H. Wang, R. C. Bell, M. J. Iedema, G. K. Schenter, K. Wu, J. P. Cowin, *J. Phys. Chem. B* **2008**, *112*, 6379.
[33] Y. Yan, Y. Lu, C. Liu, X. Yu, C. Wang, R. Yang, S. Lin, *Sol. RRL* **2022**, *6*, 2200782.
[34] A. Abnavi, R. Ahmadi, A. Hasani, M. Fawzy, M. R. Mohammadzadeh, T. De Silva, N. Yu, M. M. Adachi, *ACS Appl. Mater. Interfaces* **2021**, *13*, 45843.
[35] S. Lin, X. Chen, Z. L. Wang, *Nano Energy* **2020**, *76*, 105070.
[36] R. Ahmadi, A. Abnavi, A. Hasani, H. Ghanbari, M. R. Mohammadzadeh, M. Fawzy, F. Kabir, M. M. Adachi, *Small* **2023**, 2304988, https://doi.org/10.1002/smll.202304988.
[37] A. J. Lopez-Garcia, O. Blazquez, C. Voz, J. Puigdollers, V. Izquierdo-Roca, A. Pérez-Rodríguez, *Sol. RRL* **2022**, *6*, 2100909.
[38] N. Ma, Y. Yang, *Nano Energy* **2017**, *40*, 352.
[39] D. You, C. Xu, W. Zhang, J. Zhao, F. Qin, Z. Shi, *Nano Energy* **2019**, *62*, 310.
[40] A. Abnavi, R. Ahmadi, H. Ghanbari, M. Fawzy, A. Hasani, T. De Silva, A. M. Askar, M. R. Mohammadzadeh, F. Kabir, M. Whitwick, *Adv. Funct. Mater.* **2022**, *33*, 32210619.
[41] C. Lan, C. Li, Y. Yin, H. Guo, S. Wang, *J. Mater. Chem. C* **2015**, *3*, 8074.
[42] K. H. Kim, A. Späh, H. Pathak, C. Yang, S. Bonetti, K. Amann-Winkel, D. Mariedahl, D. Schlesinger, J. A. Sellberg, D. Mendez, *Phys. Rev. Lett.* **2020**, *125*, 076002.
[43] P. Wan, M. Jiang, T. Xu, Y. Liu, X. Fang, C. Kan, *Adv. Opt. Mater.* **2022**, *10*, 2101851.
[44] J. P. Silva, E. M. Vieira, K. Gwozdz, A. Kaim, L. M. Goncalves, J. L. MacManus-Driscoll, R. L. Hoye, M. Pereira, *Nano Energy* **2021**, *89*, 106347.
[45] L. Chen, B. Wang, J. Dong, F. Gao, H. Zheng, M. He, X. Wang, *Nano Energy* **2020**, *78*, 105260.
[46] M. Kumar, M. Patel, J. Kim, D. Lim, *Nanoscale* **2017**, *9*, 19201.
[47] M. Kumar, M. Patel, T. T. Nguyen, J. Kim, J. Yi, *Nanoscale* **2018**, *10*, 6928.
[48] B. D. Boruah, S. N. Majji, S. Nandi, A. Misra, *Nanoscale* **2018**, *10*, 3451.
[49] Y. Shen, X. Yan, H. Si, P. Lin, Y. Liu, Y. Sun, Y. Zhang, *ACS Appl. Mater. Interfaces* **2016**, *8*, 6137.
[50] J. Huang, Q. Li, X. Lu, J. Meng, Z. Li, *Adv. Mater. Interfaces* **2022**, *9*, 2200327.
[51] S. M. Hatch, J. Briscoe, S. Dunn, *Adv. Mater.* **2013**, *25*, 867.
[52] Z. Wang, R. Yu, C. Pan, Z. Li, J. Yang, F. Yi, Z. L. Wang, *Nat. Commun.* **2015**, *6*, 8401.
[53] Z. Yang, H. Wang, L. Guo, Q. Zhou, Y. Gu, F. Li, S. Qiao, C. Pan, S. Wang, *Small* **2021**, *17*, 2101572.
[54] H. Ghanbari, A. Abnavi, A. Hasani, F. Kabir, R. Ahmadi, M. R. Mohammadzadeh, M. Fawzy, T. De Silva, M. M. Adachi, *Nanotechnology* **2023**, *34*, 285207.
[55] J. Tan, H. Nan, Q. Fu, X. Zhang, X. Liu, Z. Ni, K. Ostrikov, S. Xiao, X. Gu, *Adv. Electron. Mater.* **2022**, *8*, 2100673.
[56] C. Jia, D. Wu, E. Wu, J. Guo, Z. Zhao, Z. Shi, T. Xu, X. Huang, Y. Tian, X. Li, *J. Mater. Chem. C* **2019**, *7*, 3817.
[57] P.-Y. Huang, H.-J. Chen, J. Qin, L. Zhen, C. Xu, *Nanoscale Adv.* **2022**, *4*, 5290.
[58] S. Li, D. Ouyang, N. Zhang, Y. Zhang, A. Murthy, Y. Li, S. Liu, T. Zhai, *Adv. Mater.* **2023**, *35*, 2211855.
[59] A. Hasani, Q. V. Le, M. Tekalgne, M.-J. Choi, T. H. Lee, H. W. Jang, S. Y. Kim, *NPG Asia Mater.* **2019**, *11*, 47.
[60] Q. Li, J. Song, F. Besenbacher, M. Dong, *Acc. Chem. Res.* **2015**, *48*, 119.

© 2024 The Authors. Advanced Optical Materials published by Wiley-VCH GmbH

21951071, 0, Downloaded from https://onlinelibrary.wiley.com/doi/10.1002/adom.202302651 by Simon Fraser University, Wiley Online Library on [07/02/2024]. See the Terms and Conditions (https://onlinelibrary.wiley.com/terms-and-conditions) on Wiley Online Library for rules of use; OA articles are governed by the applicable Creative Commons License